Tribological Properties of Self-Lubricating Polymer–Steel Laminated Composites

Article *in* Tribology Transactions · November 2013

DOI: 10.1080/10402004.2013.805348

CITATIONS
9

READS
307

5 authors, including:

Guangneng Dong
Xi'an Jiaotong University
185 PUBLICATIONS **3,012** CITATIONS

SEE PROFILE

Qunfeng Zeng
Xi'an Jiaotong University
131 PUBLICATIONS **1,814** CITATIONS

SEE PROFILE

Tribology Transactions

ISSN: 1040-2004 (Print) 1547-397X (Online) Journal homepage: http://www.tandfonline.com/loi/utrb20

Tribological Properties of Self-Lubricating Polymer–Steel Laminated Composites

Dong-Ya Zhang , Peng-Bo Zhang , Ping Lin , Guang-Neng Dong & Qun-Feng Zeng

To cite this article: Dong-Ya Zhang , Peng-Bo Zhang , Ping Lin , Guang-Neng Dong & Qun-Feng Zeng (2013) Tribological Properties of Self-Lubricating Polymer–Steel Laminated Composites, Tribology Transactions, 56:6, 908-918, DOI: 10.1080/10402004.2013.805348

To link to this article: http://dx.doi.org/10.1080/10402004.2013.805348

Accepted online: 20 Jun 2013.

Tribology Transactions, 56: 908-918, 2013

ISSN: 1040-2004 print / 1547-397X online
DOI: 10.1080/10402004.2013.805348

Tribological Properties of Self-Lubricating Polymer–Steel Laminated Composites

DONG-YA ZHANG, PENG-BO ZHANG, PING LIN, GUANG-NENG DONG, and QUN-FENG ZENG
Key Laboratory of Education Ministry for Modern Design and Rotor-Bearing System
Xi'an Jiaotong University
Xi'an 710049, P.R. China

Self-lubricating polymer–steel laminated composites (SLC) consisting of matrix zones and filled zones were fabricated by a laminating–bonding process. The matrix zones were silicon steel sheets and the filled zones were polymer matrix filled with MoS_2 and graphite, respectively. The control specimen was prepared by spraying a polymer composite coating on a GCr15 disc. The tribological properties of SLC were investigated using a ball-on-disc tribometer under different loads and frequencies. Compared to the control specimen, the friction coefficient and wear rate of SLC was reduced by 57% and threefold at 4 N and 6 Hz, respectively. In addition, the friction coefficient of SLC was low and stable under low reciprocating frequency, and it was high and fluctuating under high reciprocating frequency. In addition, the wear rate increased with increasing applied load and reciprocating frequency. Scanning electron microscopy (SEM) images show that the lubricating mechanism of SLC was that solid lubricants embedded in filled zones expanded and smeared a layer of transfer film on the sliding path to lubricate the surface. The thermal expansion of solid lubricants was simulated using ANSYS software with thermal-stress coupling. The simulation results showed the maximum temperature of the filled zones was 130°C, and the maximum normal displacement of solid lubricants was approximately 10 μm. This confirmed that the solid lubricants expanded effectively by the aid of frictional heat.

KEY WORDS

Self-Lubricating Laminated Composites; Tribological Properties; Transfer Film; Thermal Expansion; Thermal-Stress Coupling

INTRODUCTION

Multilaminated biomaterials, such as bamboo, teeth, and shells are selected by natural evolution for their strong load-bearing property, high impact resistance, and low density. As a typical multilaminated biomaterial, shells were composed of 95–99 wt% aragonite calcite and 1–5 wt% organic components (Wang, et al. *(1)*), which exhibited remarkable antiwear properties by integrating functions of the material, structure, and morphology. Jia, et al. *(2)* reported that organic components of bivalve shells were transferred to the friction surface and formed an organic film, which lubricated and protected the friction surface. Tong, et al. *(3)* found that the shells had a low friction coefficient under low load and velocity, and the dominant wear mechanisms were stress fatigue and three-body abrasive wear. Leung and Sinha *(4)* found that the shells had good scratch resistance, because an organic matrix with low yield stress existed between the laminated structures and served as good crack deflecting structures, thus preventing severe wear when the cracks initiated. Moreover, Stempfle, et al. *(5)* revealed that when the contact pressure was below 0.4 MPa, wear was mild because the frictional heat was insufficient to degrade the organic components. However, the frictional temperature under higher contact pressure was over the melting point of the organic components, increasing wear of shells.

Inspirations from biomaterials have led to the development of artificially laminated composites, and a few researchers have investigated the tribological properties of the laminated composites. Ceramic matrix–laminated composites with low specific density and high hardness have been widely applied as tribological materials. Toschi, et al. *(6)* and Bueno, et al. *(7)* enhanced the toughness of ceramic-laminated composites by combining laminations with thermal expansion coefficients, and the wear resistance was enhanced. The wear resistance of Si_3N_4–%TiN multilayer laminates (Hadad, et al. *(8)*) was enhanced three times by adding 30% TiN to the silicon nitride matrix. Deng *(9)* prepared a laminated nozzle by hot pressing and noted that the laminated nozzles with 2% (W, Ti) C between adjacent layers exhibited higher erosion wear resistance. However, the friction coefficients of those laminated composites are very high under dry sliding, and their applications are limited.

An effective strategy being employed to reduce friction coefficient is the formation of a transfer film. Many studies have shown that transfer films formed on the friction surface have low shear strength and a lubricating effect (Ji, et al. *(10)*; Hu and Hu *(11)*). Thus a soft component or solid lubricants are used as filling materials to fabricate self-lubricating laminated composites. Metal molybdenum (Qi, et al. *(12)*) was added into the

Manuscript received December 19, 2012
Manuscript accepted May 10, 2013
Review led by Cris Schwartz

laminated system to fabricate self-lubricating Al_2O_3/Mo-laminated composites, and the metal molybdenum was oxidized under high temperature and formed an MoO_3 lubricating film on the sliding surface, which reduced the friction coefficient of the Al_2O_3/Mo-laminated composites at 800°C. For polymer matrix laminated composites, Mondelin, et al. *(13)* reported that the friction coefficient of carbon fiber–reinforced polymer laminate was insensitive to sliding velocity or contact pressure. Zhao, et al. *(14)* fabricated Polyimide/fluorinated ethylene propylene (PI/FEP)-laminated composites using a hot pressing process, and the results showed the polymer-laminated composites had a lower friction coefficient and higher wear rate under water lubrication compared with dry sliding. B. C. Kim, et al. *(15)* and S. S. Kim, et al. *(16)* obtained carbon epoxy–laminated composites with a grooved surface and the composite surface significantly improved the wear resistance because a lubricating film was formed on the contact region during dry friction. They also implied that laminated composites with a high volume fraction of carbon fiber had a lower friction coefficient.

The incorporation of solid lubricants in a multilayer architecture is one of the innovative strategies being employed to improve the mechanical and tribological properties of polymer–steel laminated composites. Matrix zones offer remarkable load-bearing capacity and filled zones consisting of solid lubricants reduce the friction force and trap wear debris. In this study, a process of fabricating self-lubricating polymer–steel laminated composites (SLC) was introduced; silicon steel sheets were provided as matrix zones and the filled zones were composed of a polymer matrix filled with solid lubricants. In addition, the effects of reciprocating frequencies and applied loads on the tribological properties of SLC were studied. The wear and lubricating mechanisms were analyzed using scanning electron microscopy (SEM) and energy-dispersive analysis (EDS). Moreover, the thermal expansion of solid lubricants in filled zones was analyzed using finite element method simulations.

EXPERIMENTAL PROCEDURES

The polymer matrix was epoxy resin E51 with an epoxide-equivalent molecular weight of 210–250 g/mol (Wuxi Resin Factory of Bluestar New Chemical Materials Co. Ltd., China) cured with low-molecular-weight polyamine 650 (Haitian Chemical Reagent Co. Ltd., China). MoS_2 and graphite powders with an average particle size of 0.5 μm were applied as solid lubricants. Silicon steel sheets (elastic modulus, E = 150 GPa; Poisson's ratio, $\nu = 0.24$) with a thickness of 0.2 mm and length of 40 mm were adopted as matrix material.

Figure 1 illustrates the fabrication process for polymer–steel laminated composites. First of all, silicon steel sheets with heights of 30 and 25 mm were prepared and cleaned in an ultrasonic bath of acetone for 30 min and then dried at 100°C for 1 h and cooled down to room temperature. The filling material was composed of 50 wt% epoxy resin, 5 wt% graphite, 20 wt% MoS_2, 20 wt% polyamide, and 5 wt% butanone. Before laminating, epoxy resin was uniformly sprayed on both surfaces of the silicon steel sheets. Laminated composites with

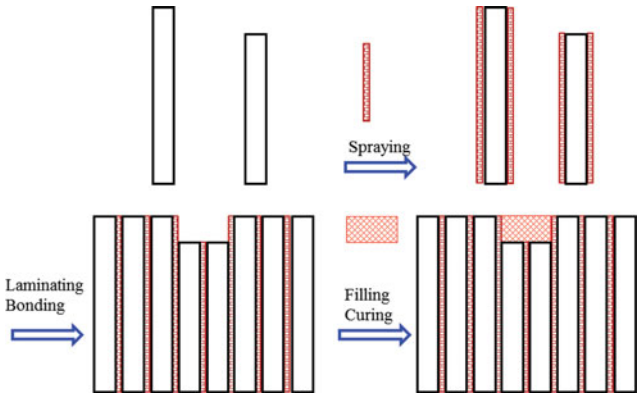

Fig. 1—Schematic diagram of the fabrication of SLC (color figure available online).

regular microgrooves were fabricated by laminating different heights of silicon steel sheets together, and the laminates were cured at 100°C for 2 h. Filling materials were filled into the grooves to prepare self-lubricating laminated composites, and then the SLC was cured at 120°C for 2 h. Finally, redundant filling materials were polished until the steel surface was exposed. A GCr15 control specimen with a 60-μm coating was prepared by spraying polymer composites. In addition, the formulation of the polymer composites and filling materials in SLC is the same.

Thermal gravimetric (TG) analysis of the filling materials was performed using a TG apparatus (Netzsch Sta 409 PC/PG, Germany). The specimen was heated at a heating rate of 10°C/min from room temperature to 600°C in an argon atmosphere, and the argon flow during the experiments was 100 mL/min.

Linearly reciprocating ball-on-disc friction and wear tests were performed on a UMT-2 tribometer (CETR Co., Ltd.) according to ASTM standard G133-05 (ASTM International *(17)*). The lower specimen was SLC with a size of 40 mm × 20 mm × 30 mm. The upper specimen was a 440C steel ball with a diameter of 9.5 mm and hardness of HRC 60–63. The sliding direction of the lower specimen was perpendicular to the grooves. The test conditions are listed in Table 1. Before testing, all specimens were polished to $Ra = 0.1$ μm; the disc specimens were cleaned with alcohol wipes, and the steel balls were ultrasonically cleaned in acetone for 5 min and then dried in hot air.

Wear was described by the volume loss of the disc specimens. The wear scar profile was acquired by means of a surface profiler. The wear scar width and depth were measured from the profile curve and the cross-section area was calculated. The wear scar

TABLE 1—TRIBOLOGICAL TEST CONDITIONS

Applied load (N)	4, 6, 8, 10
Reciprocating frequency (Hz)	4, 6, 8
Stroke (mm)	6
Lubrication type	Dry
Test time (min)	30, 45
Temperature (°C)	25
Relative humidity (%)	40–45

was measured at four different locations. From the cross-section area the wear volume was integrated around the scar length. The wear rate k (mm^3/N m) was calculated as follows (Zhang, et al. *(18)*):

$$k = \frac{l\lambda\left(\arcsin\frac{b_1}{2r}r^2 - \frac{b_1\sqrt{4r^2-b_1^2}}{4}\right) + l(1-\lambda)\left(\arcsin\frac{b_2}{2r}r^2 - \frac{b_2\sqrt{4r^2-b_2^2}}{4}\right)}{P \times S}, \quad [1]$$

where r is the radius of the ball (4.75 mm), $\lambda = 0.4$, l is the reciprocating stroke (6 mm), b_1 is the wear scar width on the matrix zone (mm), b_2 is the wear scar width on the filled zone (mm), S is the sliding distance (m), and P is the applied load (N).

After testing, the wear scars were observed using a JSM-6460 SEM. Before SEM observation, a 30-nm gold film was deposited on the disc to enhance the electrical conductivity of the filled zones. The surface chemical compositions of the disc were examined by an INCA Energy + EDS (Oxford, UK).

RESULTS AND DISCUSSION

Microstructure of SLC

The microstructures of the laminated composites are shown in Fig. 2. As shown in Fig. 2a, marker A is the silicon steel sheet, called the *matrix zone*, and marker B is the solid lubricant, called the *filled zone*. It can be seen that SLC has a uniform appearance without cracks. Figure 2b shows the transverse cross section of SLC; the filled zones are uniformly distributed and the filled depth is approximately 5 mm. As shown in Fig. 2, the filled zones are tightly bonded to the metal substrate. Elemental compositions of regions A and B are given in Table 2. Mo, O, and S are undetected in the matrix zones, indicating that solid lubricants are wiped off from the matrix zones.

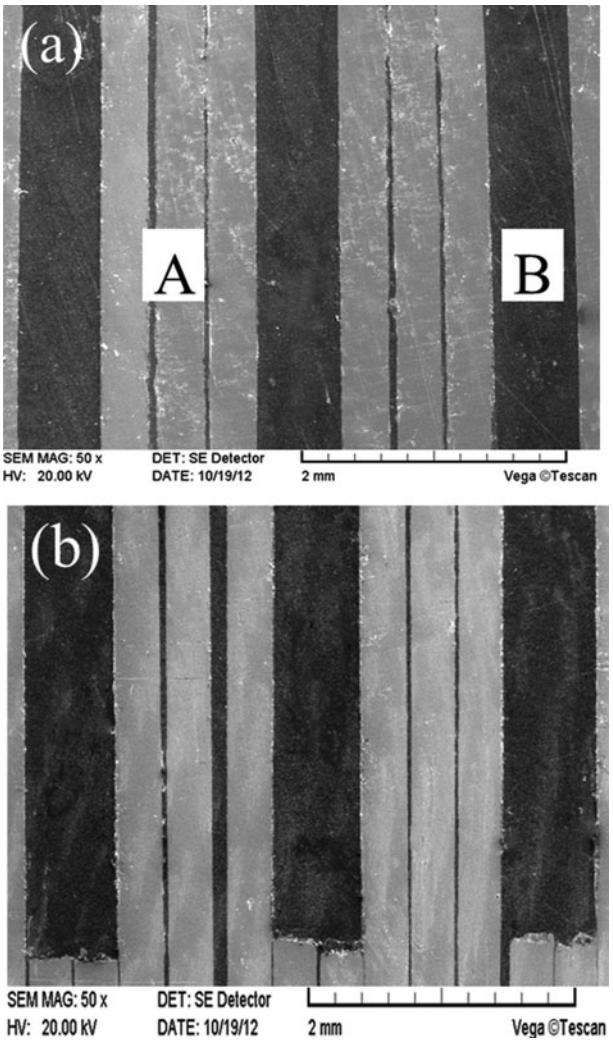

Fig. 2—Microstructure of SLC: (a) parallel section view and (b) cross-sectional view.

Thermal Property of the Filling Materials

The thermal properties of the filling materials are shown in Fig. 3. The TG curve shows that the specimen has undergone two stages of mass loss. The first stage of degradation occurs in the temperature range of 30–260°C with a weight loss of 1.87 wt%, which is attributed to the removal of hygroscopic water and easily volatile molecules. The second stage of degradation occurs in the temperature range of 260–390°C with a weight loss of 46.59 wt%. In addition, a large amount of gases with small molecules such as CO and CO_2 are released in this range (Zhang, et al. *(19)*). As a result, the temperature range of 260–390°C is considered the key temperature range for thermal decomposition of the filling material. Whereas in the temperature range of 390–600°C the mass loss rate increases slowly with increasing temperature, the TG curve becomes flat after 500°C, which may be due to residual carbonization, MoS_2, or graphite.

Tribological Properties of SLC

In order to highlight the tribological properties of SLC, a control specimen and SLC are tested under the same test conditions. Figure 4a shows the variation in friction coefficient with sliding time at an applied load of 6 N and reciprocating frequency of 4 Hz. The friction coefficient of the control specimen is 0.20 in the initial stage and then quickly increases to a steady value of 0.26. In the case of SLC, the friction coefficient is stable and as low as 0.16, which is 50% lower than that of the control specimen. It can be seen that the friction coefficient of SLC is much lower than that of self-lubricating polymer composite coating during the dry sliding test. Friction behavior also has a strong influence on the wear properties, and the wear rate of self-lubricating polymer coating is 4.3 times higher than that of SLC, as shown in Fig. 4b, which indicates that SLC has an excellent wear resistance.

Self-lubricating polymer composite coating has a relatively high friction coefficient and poor load-bearing capacity due to its inadequate adhesion and low thermal conductivity (Biswas and

TABLE 2—EDS ANALYSIS OF ELEMENTS (WT%) IN DIFFERENT REGIONS

Region	C	O	S	Mo	Si	Fe
A	1.45	—	—	—	2.58	95.97
B	76.51	1.43	10.34	11.72	—	—

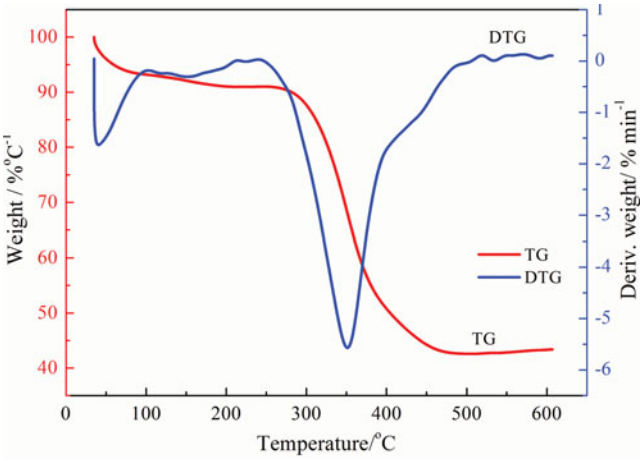

Fig. 3—Thermal property of the filling materials (color figure available online).

Satapathy *(20)*; Öztürk, et al. *(21)*). On the contrary, SLC, with a multilayer structure, improves the tribological properties by providing solid lubricants embedded in the filled zones, and the matrix zones enhance the load-bearing capacity of SLC under high contact pressure. Therefore, the tribological properties of SLC are improved.

Influence of Reciprocating Frequency

Figure 5a shows the friction coefficient with a sliding frequency of 4 Hz and applied loads of 4 and 6 N after sliding 130 m. The friction coefficients of SLC are very steady at the beginning of the tests. To be specific, the friction coefficient begins with a low value at the initial stage and quickly increases to a steady state (in the range of 0.13–0.14) at an applied load of 4 N. Similar behavior is observed at 6 N: the friction coefficient is 0.14 at steady state and increases 14% compared to that at 4 N. In addition, the friction coefficients are lower than 0.17 at 4 and 6 N. These findings suggest that SLC demonstrates a self-lubricating property under low reciprocating frequency. When the reciprocating frequency increases to 6 Hz, the friction coefficients fluctuate smoothly in the range from 0.15 to 0.17 for a sliding distance of 90 m at 4 and 6 N (Fig. 5b). However, the friction coefficients increase sharply and fluctuate evidently with prolonged sliding distance; in addition, the friction coefficient increases dramatically from 0.14 to 0.28 after sliding 110 m at an applied load of 4 N. The

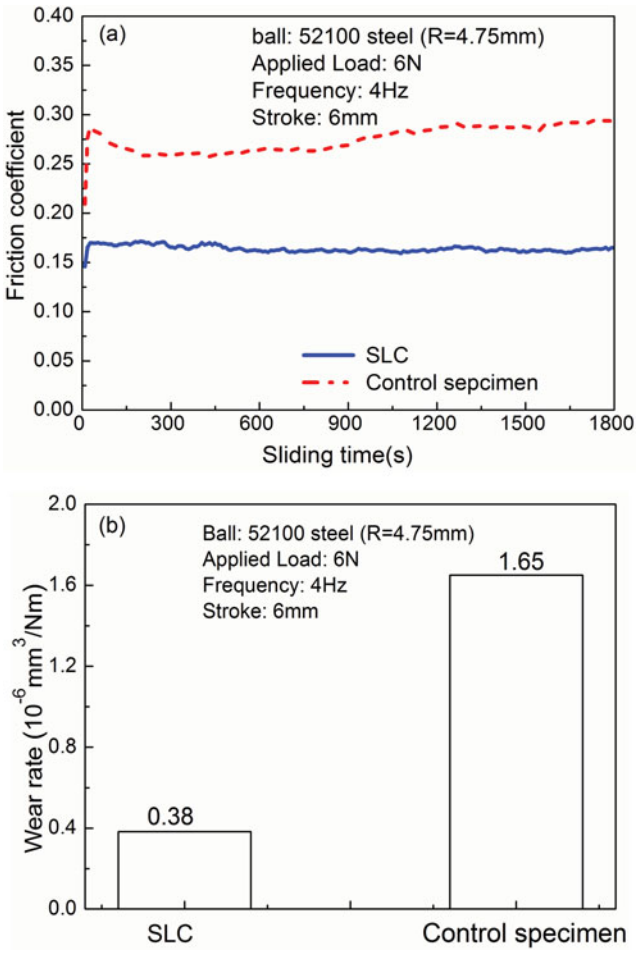

Fig. 4—Tribological behavior: (a) friction coefficient and (b) wear rate (color figure available online).

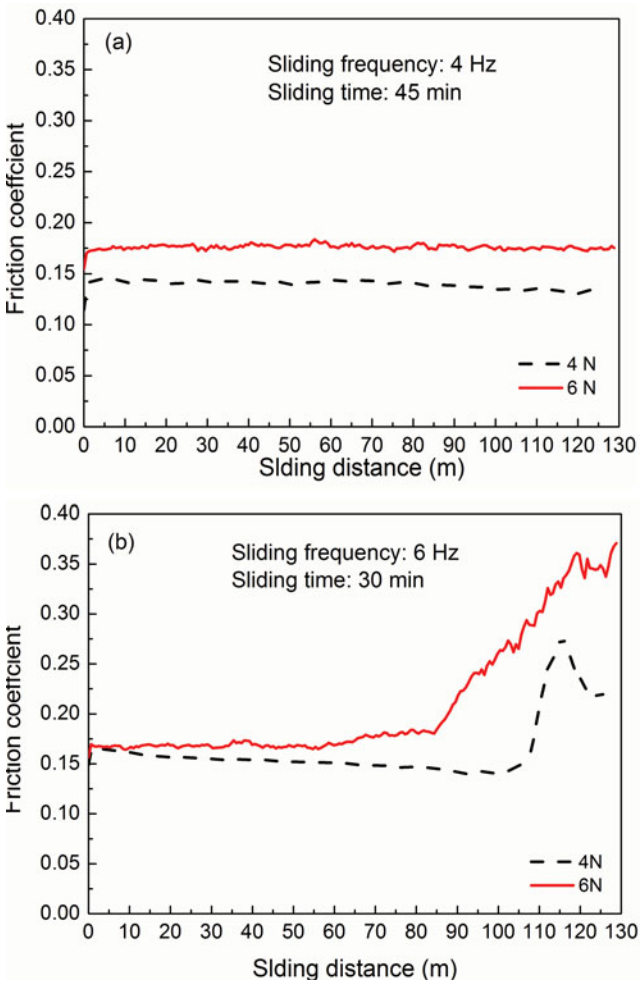

Fig. 5—Effect of reciprocating frequency on friction coefficient: (a) 4 Hz and (b) 6 Hz (color figure available online).

friction coefficient increases sharply from 0.17 to 0.38 after sliding 90 m at 6 N. High sliding frequency results in large fluctuations in the friction coefficient, and the friction coefficient increases with increasing sliding frequency. This is because with increasing reciprocating frequency, the contact interface temperature between the ball and disc generally increases due to the frictional heat and results in a decrease in the elastic modulus of polymer at higher temperature (Li, et al. *(22)*; Meng, et al. *(23)*). Consequently, the influence of reciprocating frequency on the tribological properties is significant, and a low reciprocating frequency is more beneficial for improving the tribological properties of SLC.

Influence of the Applied Load

Figure 6a shows the variation in the average friction coefficient of SLC with increasing applied load at the reciprocating frequency of 4–8 Hz. The average friction coefficient curve firstly increases and then decreases with increasing applied load at 4 Hz, whereas the average friction coefficient has an abrupt increase in the initial stage and then decreases with increasing applied load at 6 Hz. As the reciprocating frequency increases to 8 Hz, the average friction coefficient shows an abrupt decrease initially and then increases with increasing applied load. It is evident that the average friction coefficient curves fluctuate widely under high reciprocating frequency, which indicates that the friction coefficient of SLC is sensitive to variations in applied load under high reciprocating frequency.

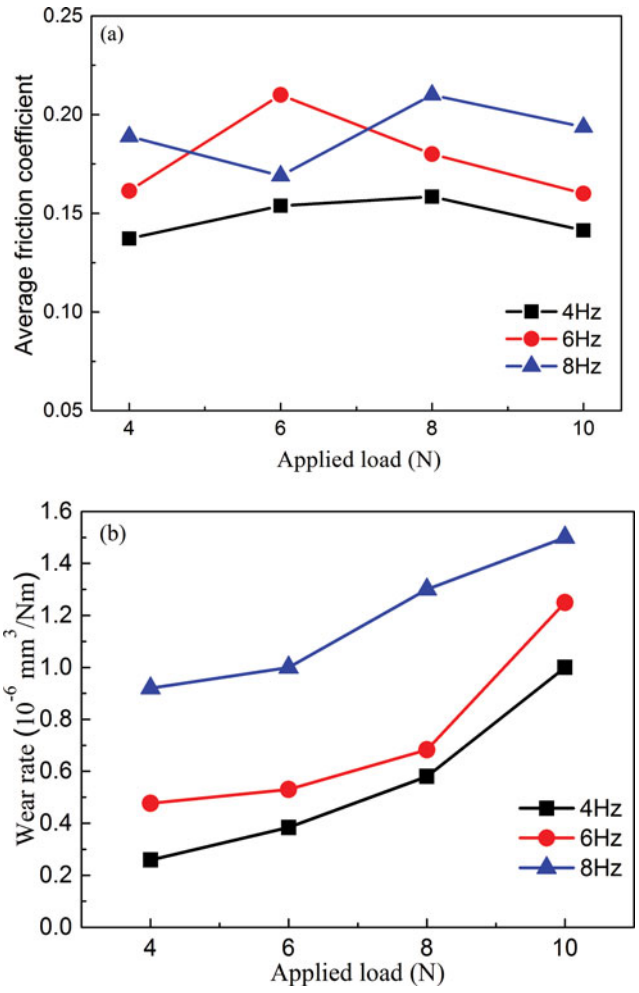

Fig. 6—Effect of applied load on (a) average friction coefficient and (b) wear rate of SLC (color figure available online).

Figure 6b represents the variation in wear rate of SLC with applied load at reciprocating frequencies of 4, 6, and 8 Hz. It is found that wear rate of the SLC are in the magnitude of 10^{-6} mm^3/N m. The wear rate increases as the applied load increases. This is in agreement with studies by other researchers (Liza, et al. *(24)*; Zhang, et al. *(25)*). In addition, the increase in reciprocating frequency increases the wear rate. A low wear rate is obtained at low applied load; however, as the load increases to 10 N, the wear rate increases rapidly. At a reciprocating frequency of 4 Hz, the wear rate at 10 N is three times higher than that at 4 N, and the wear rate at 8 N is two times higher than that at 4 N as the reciprocating frequency increases to 8 Hz. These results indicate that the wear resistance of SLC becomes worse under high applied load and high reciprocating frequency.

Lubricating and Wear Mechanism of SLC

To better understand the lubricating and wear mechanisms of SLC, wear scars on the matrix zones and filled zones were examined by SEM, and the element distribution in the wear scars were detected by EDS.

Figure 7 shows the EDS spectrograms of the wear scar in the matrix zones and filled zones for a load of 6 N and 4 Hz. The peaks of C, Mo, and S are observed in the matrix zone (as shown in Fig. 7a), whereas Mo, S, or a low-density C peak is undetected before the friction test (as shown in Table 2). This reveals that elements of C, Mo, and S are from filled zones, and these chemical elements appear in the matrix zone because solid lubricants in filled zones are smeared and reorganized due to friction. Accordingly, the EDS results indicate that MoS_2 and graphite are effectively replenished and a transfer film is formed on the contact zone. Figure 7b shows that high-intensity C, Mo, and S peaks and a low-intensity Fe peak are detected on filled zones; the low intensity of the Fe peak indicates the steel wear debris trapped by filled materials during dry sliding. MoS_2 and graphite are widely applied as effective filling materials and the sufficient supplement of MoS_2 and graphite greatly reduced the friction coefficient and enhanced wear resistance (Hu, et al. *(26)*). Hence, the tribological properties of SLC are improved by the addition of solid lubricants.

Wear Scar on Matrix Zones

Figure 8 shows SEM images of wear scars in the matrix zones under a reciprocating frequency of 4 Hz after sliding 130 m. The transfer film is uniformly distributed on the matrix zones, and Mo, S, and C elements are examined on the matrix zones (as previously shown in Fig. 7b). This is because solid lubricants embedded in filled zones are thermally expanded and transferred to the contact zone, and form a transfer film. Frictional heat caused by high contact pressure accelerates the expansion of solid lubricants, which results in a uniform and continual transfer film forming in the contact zone. In addition, there is slight wear debris on the worn surface along the sliding path at a load of 4 N (Fig. 8a),

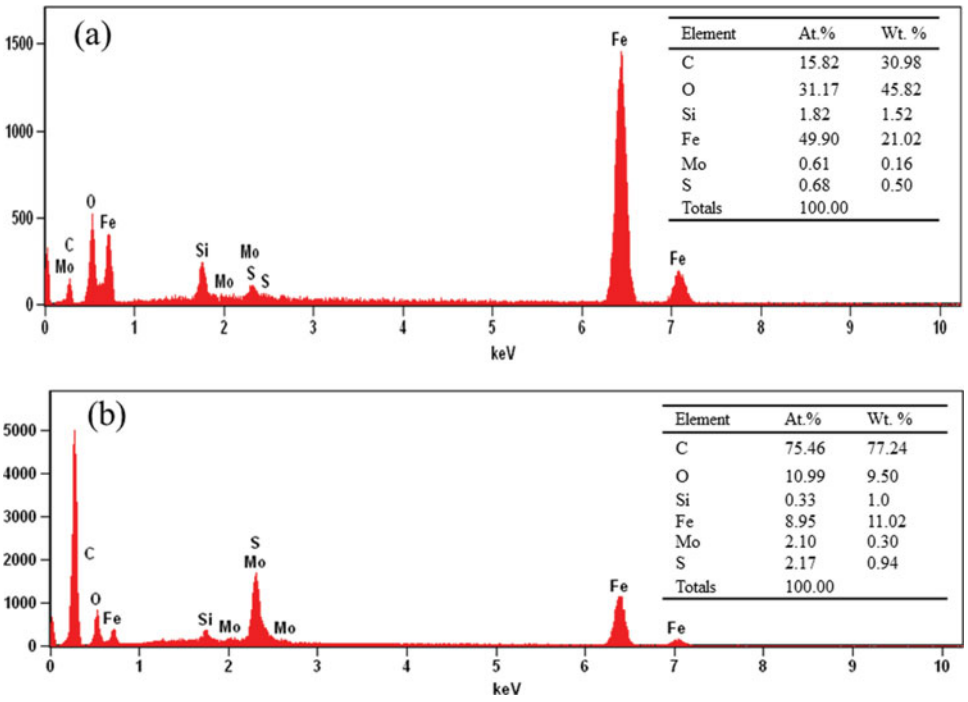

Fig. 7—EDS analysis of the wear scar: (a) matrix zones and (b) filled zones at 4 N, 6 Hz (color figure available online).

and large wear debris is observed on the worn surface at a load of 6 N (Fig. 8b). This demonstrates that the wear mechanism of the matrix zone under low reciprocating frequency is adhesive wear.

Figure 9 shows SEM images of wear scars in the matrix zones under a reciprocating frequency of 6 Hz after sliding 130 m. A discontinuous transfer film in the matrix zones, smooth grooves, significant wear debris, and light plastic deformation appeared on the worn surface at 4 N (Fig. 9a). When the applied load increases to 6 N, the transfer film is removed away from the matrix zones. Distinct plastic deformation and severe plowing are the wear mechanisms of SLC under high frequency and applied load (Fig. 9b). This indicates that the transfer film may wear out and induces the lubricating failure of SLC under high load and reciprocating frequency.

Wear Scar on Filled Zones

Figure 10 shows SEM images of wear scars in the filled zones under a reciprocating frequency of 4 Hz after sliding 130 m. The morphologies of the wear scars at 4 and 6 N are similar, and the surfaces covered with wear debris, are smooth. In addition, the width of the wear scar at 6 N (Fig. 10b) is almost 1.5 times larger than that at 4 N. The reason may be that polymer material is torn away by the ploughing of the sliding ball, and the wear mechanism of filled zones under low reciprocating frequency is adhesive wear.

Figure 11 shows the SEM images of wear scars on the filled zones under a reciprocating frequency of 6 Hz after sliding 130 m. The wear scars with adhesion and plastic deformation are smooth at 4 N (Fig. 11a), and significant plastic deformation, flake pits, and microcracks are displayed in the wear scar at 6 N (Fig. 11b). Moreover, it is evident that wear on the worn surface at 6 N is severe compared to that at 4 N, indicating that the wear type changes from abrasive wear to fatigue wear. The results can be explained as follows: firstly, significant frictional heat accumulates on the contact surface under high contact pressure, and the hardness and strength of polymer decrease under frictional heat, which accelerates wear. Secondly, under the effect of repeated cyclic stress, severe deformation of the filled materials occurs, and the filled materials are fatigue and the micro-cracks are formed on the SLC surface with the sliding continues. Consequently, the dominant wear mechanism of filled zones is fatigue wear under high reciprocating frequency and applied load.

Numerical Simulation

As previously described, solid lubricants embedded in the filled zones are thermally expanded and smeared on the sliding track and then form a transfer film to lubricate and protect the surface. To confirm this conclusion, a finite element method is used to simulate the thermal expansion behavior of solid lubricants under the contact pressure of 450 MPa and velocity of 36×10^{-3} m/s.

To formulate the transient temperature field, the following assumptions are made: (1) plastic deformation and wear of the filling material are independent of the heat flow behaviors so that the conservative law of energy is applicable in temperature prediction. (2) Polymer composites in the filled zones are homogeneous, and properties such as thermal conductivity, thermal diffusivity, heat capacity, and density are invariant with heat flow behaviors. In addition, there is no phase transformation throughout the process (Dong, et al. *(27)*). (3) The friction coefficient remains constant during sliding.

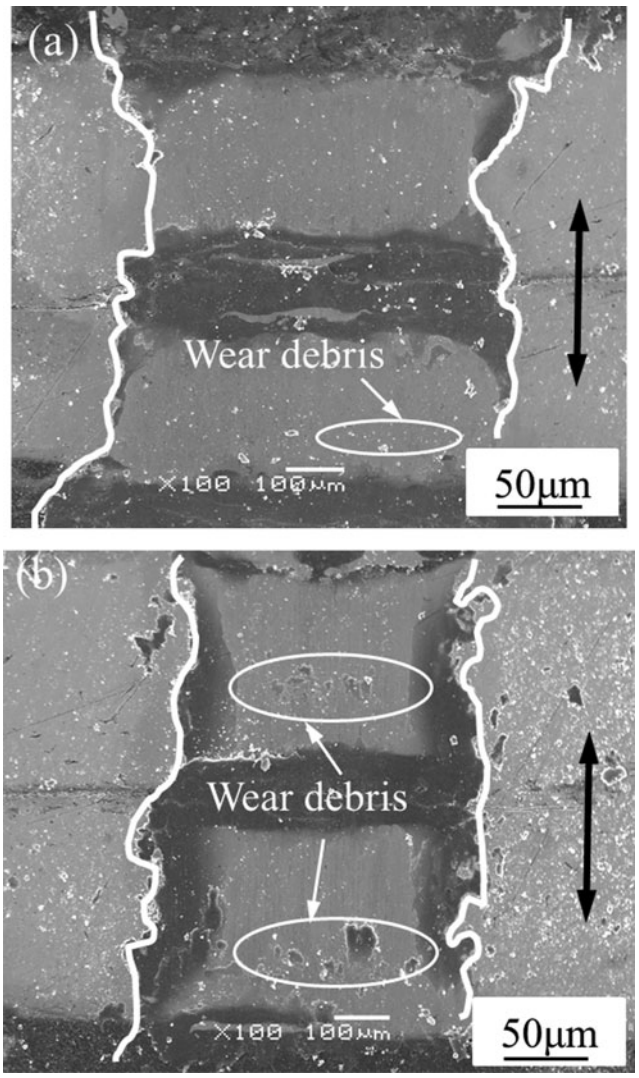

Fig. 8—SEM images of wear scars in the matrix zones at (a) 4 Hz, 4 N and (b) 4 Hz 6 N.

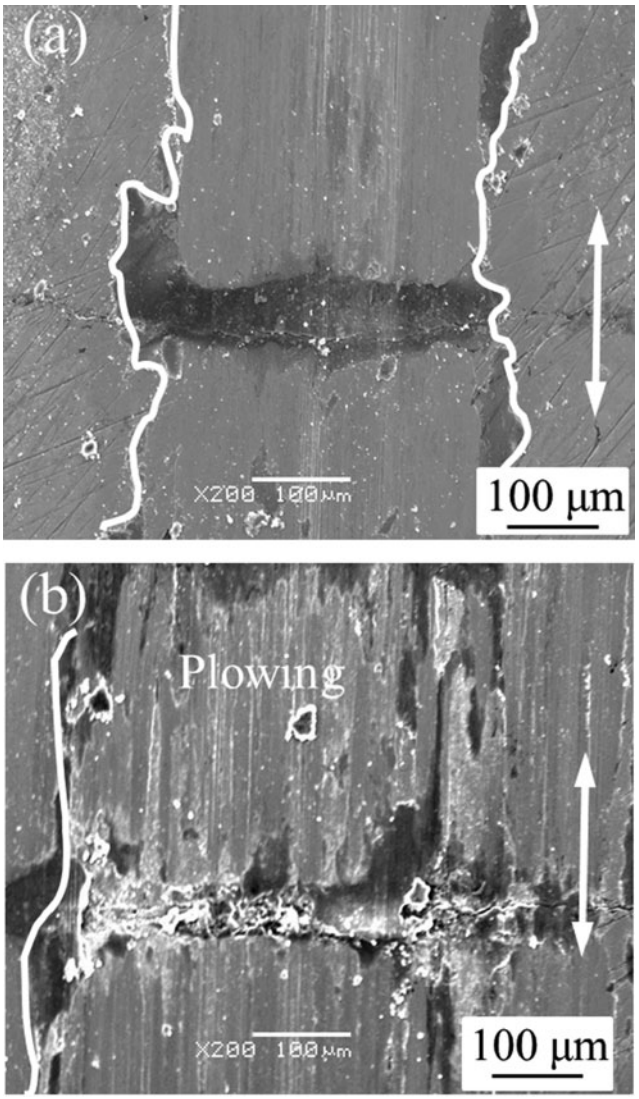

Fig. 9—SEM images of wear scars in the matrix zones at (a) 6 Hz, 4 N and (b) 6 Hz, 6 N.

Heat Conduction Equation

A Cartesian coordinate system is used to analyze the heat conduction between a ball and disc, and the governing equation for the transient three-dimensional heat conduction is expressed as (Zhang, et al. *(28)*):

$$\frac{1}{\alpha}\left(\frac{\partial^2 T}{\partial x^2}+\frac{\partial^2 T}{\partial y^2}+\frac{\partial^2 T}{\partial z^2}\right)=\frac{\partial T}{\partial t}(\Omega), \qquad [2]$$

where $a = \lambda/\rho c$ is the thermal diffusivity (m^2/s), λ is the thermal conductivity (W/m K), c is the specific heat (J/kg K), ρ is the density (kg/m^3), T is the instantaneous temperature (K), and t is the sliding time (s).

Boundary Conditions

Figure 12 shows the thermal load and convective conditions used in the model. During sliding, the frictional heat source at the interface is treated as a thermal load boundary for the ball and disc. The boundary conditions can be specified as follows:

$$\lambda\frac{\partial T}{\partial z}=-[1-g(t)]h_{d1}(T-T_0)+g(t)q(t)$$

$$\mathrm{g(t)}=\begin{cases}1 \text{ in the domain of contant zone}\\ 0 \text{ out of the domain of contact zone}\end{cases} \qquad (S_1)$$

[3]

$$\lambda\frac{\partial T}{\partial z}=\mathrm{T_0(S_2,\ S_5)} \qquad [4]$$

$$\lambda\left(\frac{\partial T}{\partial x}n_x+\frac{\partial T}{\partial y}n_y\right)=\mathrm{T_0(S_3,\ S_4,\ S_6)}, \qquad [5]$$

where $q(t)$ is the heat flux transmitted to the disc from the contact area (W/m^2), T_0 is the ambient temperature, and h_{d1} is the convective coefficient (W/m^2 K).

Thermal analysis of the filled zones requires an accurate determination of the total frictional heat generated and how the energy is distributed. During friction, some frictional heat escapes into

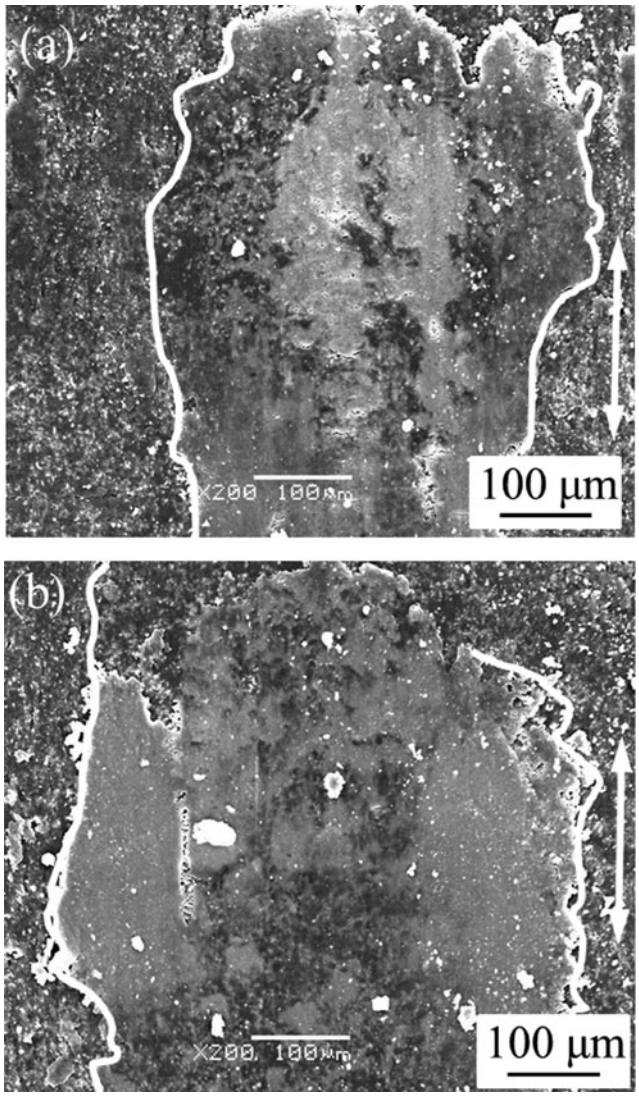

Fig. 10—SEM images of wear scars in the filled zones at (a) 4 Hz, 4 N and (b) 4 Hz, 6 N.

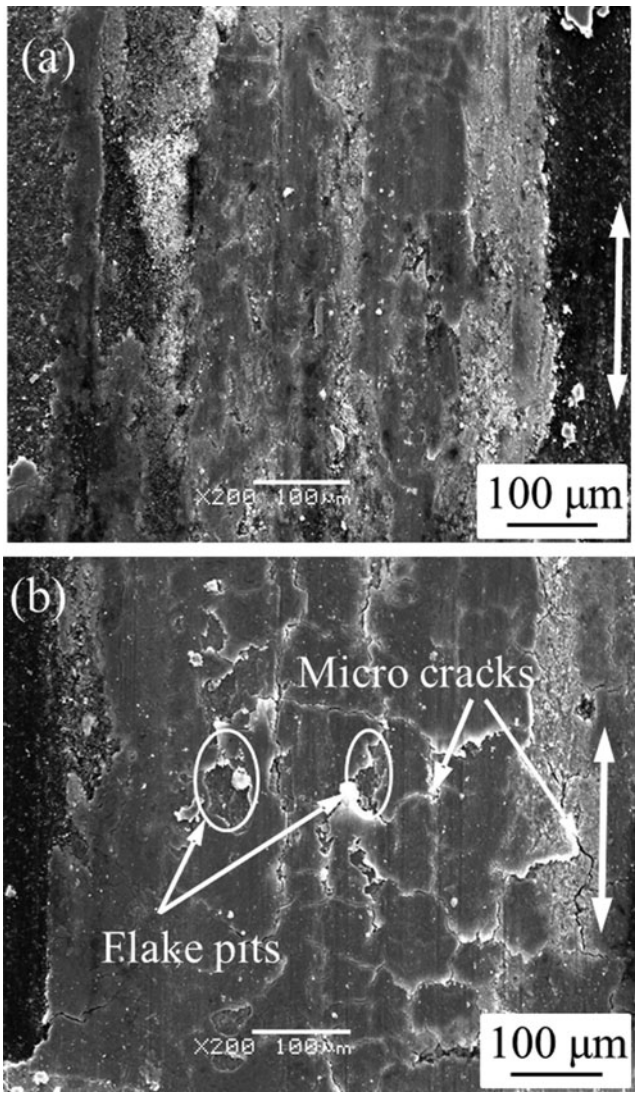

Fig. 11—SEM images of wear scars in the filled zones at (a) 6 Hz, 4 N and (b) 6 Hz, 6 N.

the air by convection and radiation (the radiation is omitted as the sliding velocity is low). The total heat generated at the interface is equal to the heat absorbed by the ball and disc. Thus, $q(t)$ can be calculated from the following equation (Mu, et al. *(29)*):

$$q(t) = \gamma \mu p v, \quad [6]$$

where $\mu = 0.15$ is the average friction coefficient of SLC taken from the experiment, $p = 450$ MPa (contact pressure of 4 N applied on a 9.5-mm steel ball), $v = 36 \times 10^{-3}$ m/s, and γ is the heat partition coefficient, which is given as (Laraqi, et al. *(30)*):

$$\gamma = \frac{1}{1 + \sqrt{\rho_1 c_1 k_1 / \rho_2 c_2 k_2}}, \quad [7]$$

where $\gamma = 0.33$, ρ is the density, c is the specific heat, and k is the thermal conductivity. Indices 1 and 2 denote the ball and disc, respectively.

Thermal-Stress Coupling

To simplify the calculation, non-line elastic deformation of the filled material is assumed and the constitutive equation of the filled materials is

$$\sigma = D(\varepsilon - \alpha \cdot \Delta T), \quad [8]$$

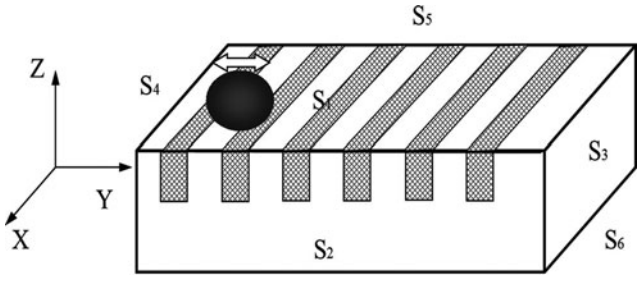

Fig. 12—Schematic of boundary conditions for the model.

where σ is the stress vector, ε is the strain vector, α is the thermal expansion coefficient vector, D is the elastic matrix, and ΔT is a variable quantity of temperature.

Simulation and Analysis Results

Based on the above assumptions, a three-dimensional finite element model is established in Fig. 13a. The mesh density of the model is controlled accurately in order to make the calculation converge to a high-precision solution, and the meshed model is shown in Fig. 13b. The physical properties of the materials are provided in Table 3.

Figure 14a shows the 3D temperature field of SLC. It can be seen that the highest and lowest temperature of the filled zones are 130 and 45°C, respectively, and a temperature gradient is distributed along the filled depth. The temperature field of the matrix zones is uniform at 38.3°C due to the matrix zones with a high coefficient of thermal conductivity. After calculation of the temperature field, the strain field is simulated with thermal-strain coupling, and the matrix zones are set as rigid bodies. The thermal-strain coupling element SOLID185 is used to simulate strain of the filling materials. The strain field of SLC is shown in Fig. 14b, and the maximum normal displacement of filling materials in the filled zones is approximately 10 μm. High temperature results in large thermal expansion of solid lubricants, and a transfer film is efficiently formed on the frictional surface.

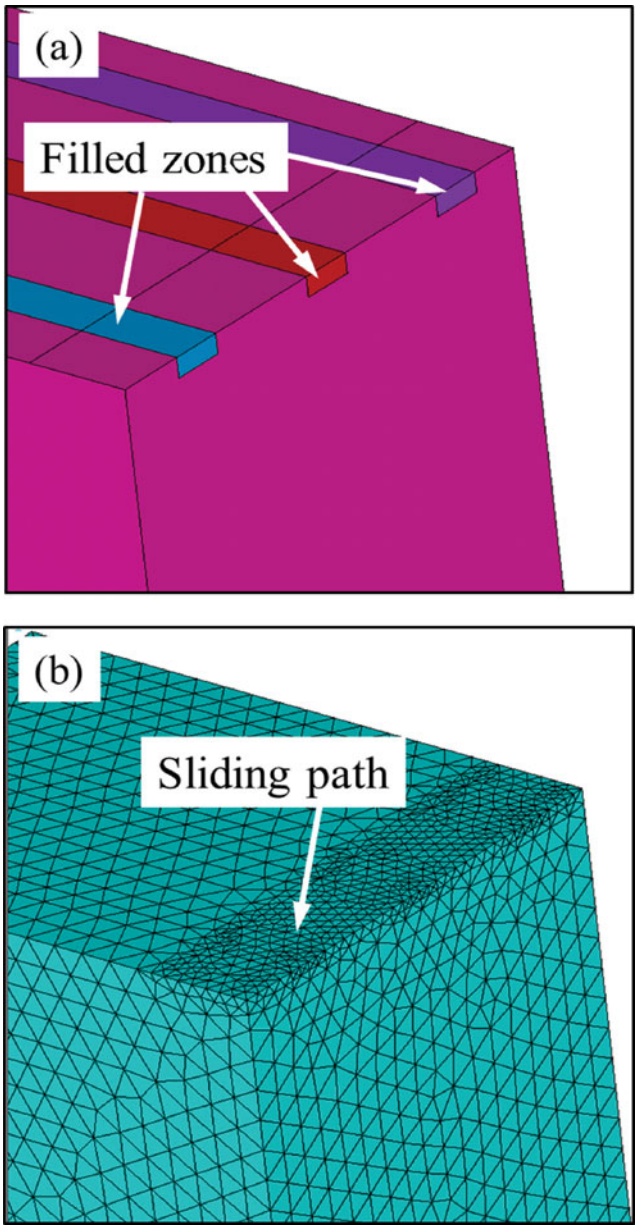

Fig. 13—(a) Geometric model and (b) meshing figure (color figure available online).

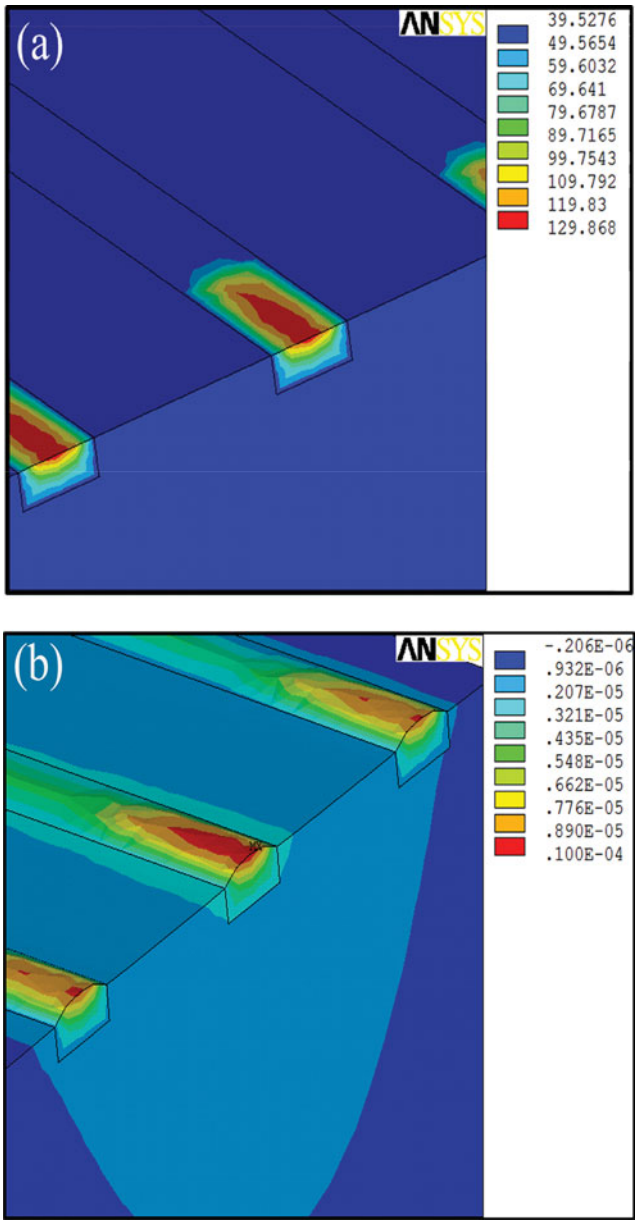

Fig. 14—Distribution of (a) temperature field and (b) strain field (color figure available online).

TABLE 3—PHYSICS PROPERTIES OF THE MATERIALS

Materials	Elastic Modulus (GPa)	Density (kg/m^3)	Conductivity (W/m K)	Specific Heat (kJ/kg K)	Thermal Expansion (e^{-6}/K)	Poisson's Ratio
Filled material	5	2,000	0.21	1.45	65.3	0.4
Matrix material	150	7,800	6.6	470	11.2	0.24

CONCLUSIONS

Polymer–steel laminated composites were fabricated by laminating–bonding process, and their tribological properties were determined under different loads and frequencies. The following conclusions can be drawn:

1. The friction coefficient and wear rate of SLC are significantly lower than that of polymer composite coating. Compared to the control specimen, the friction coefficient and wear rate of SLC decreases by 57% and threefold, respectively.
2. The friction coefficients of SLC are steady and below 0.15 at 4 Hz, whereas the friction coefficients increase sharply and fluctuate evidently with prolonged sliding distance at 6 Hz.
3. Solid lubricants embedded in filled zones are thermally expanded and then form a transfer film along the sliding track, which lubricates and protects the surface. In addition, the transfer film has a long lifetime under low reciprocating frequency and is easily damaged under high reciprocating frequency.
4. The simulation results show that the highest frictional temperature of the filled zones is about 130°C, and normal displacement of solid lubricants in the filled zones is approximately 10 μm. This indicates that a large thermal expansion of solid lubricants is caused by high frictional temperature, and thus a transfer film is efficiently formed on the contact interface.

ACKNOWLEDGEMENT

The authors appreciate the financial support from 973 Project (Grant No. 2009CB724206).

REFERENCES

(1) Wang, R. Z., Suo, Z., Evans, A. G., Yao, N., and Aksay, I. A. (2001), "Deformation Mechanisms in Nacre," *Journal of Materials Research*, **16**, pp 2485–2493.

(2) Jia, X., Ling, X. M., and Tang, D. H. (2006), "Microstructures and Friction–Wear Characteristics of Bivalve Shells," *Tribology International*, **39**, pp 657–662.

(3) Tong, J., Wang, H., Ma, Y., and Ren, L. (2005), "Two-Body Abrasive Wear of the Outside Shell Surfaces of Mollusc *Lamprotula fibrosa* Heude, *Rapana venosa* Valenciennes and *Dosinia anus* Philippi," *Tribology Letters*, **19**, pp 331–338.

(4) Leung, H. M. and Sinha, S. K. (2009), "Scratch and Indentation Tests on Seashells," *Tribology International*, **42**, pp 40–49.

(5) Stempfle, P., Djilali, T., Njiwa, R. K., Rousseau, M., Lopez, E., and Bourrat, X. (2009), "Thermal-Induced Wear Mechanisms of Sheet Nacre in Dry Friction," *Tribology Letters*, **35**, pp 97–104.

(6) Toschi, F., Melandri, C., Pinasco, P., Roncari, E., Guicciardi, S., and Portu, G. (2003), "Influence of Residual Stresses on the Wear Behavior of Alumina/Alumina–Zirconia Laminated Composites," *Journal of the American Ceramic Society*, **86**, pp 1547–1553.

(7) Bueno, S., Micele, L., Melandri, C., Baudin, C., and De Portu, G. (2011), "Improved Wear Behaviour of Alumina–Aluminium Titanate Laminates with Low Residual Stresses and Large Grained Interfaces," *Journal of the European Ceramic Society*, **31**, pp 475–483.

(8) Hadad, M., Blugan, G., Kubler, J., Rosset, E., Rohr, L., and Michler, J. (2006), "Tribological Behaviour of Si_3N_4 and Si_3N_4–%TiN Based Composites and Multi-Layer Laminates," *Wear*, **260**, pp 634–641.

(9) Deng, J. X. (2009), "Wear Behaviors of Ceramic Nozzles with Laminated Structure at Their Entry," *Wear*, **266**, pp 30–36.

(10) Ji, K. J., Shan, W. G., Xia, Y. Q., and Dai, Z. D. (2012), "The Tribological Behaviors of Self-Lubricating Composites as Filler in Copper Foam," *Tribology Transactions*, **55**, pp 20–31.

(11) Hu, T. C. and Hu, L. T. (2011), "Tribological Properties of Lubricating Films on the Al-Si Alloy Surface via Laser Surface Texturing," *Tribology Transactions*, **54**, pp 800–805.

(12) Qi, Y. E., Zhang, Y. S., and Hu, L. T. (2012), "High-Temperature Self-Lubricated Properties of Al_2O_3/Mo Laminated Composites," *Wear*, **280**, pp 1–4.

(13) Mondelin, A., Furet, B., and Rech, J. (2010), "Characterisation of Friction Properties between a Laminated Carbon Fibres Reinforced Polymer and a Monocrystalline Diamond under Dry or Lubricated Conditions," *Tribology International*, **43**, pp 1665–1673.

(14) Zhao, H., Zhang, J., Ji, T., Yang, M., Chao, M., and Kou, K. (2012), "Investigation of Tribological Properties of PI/FEP Laminated Composites under Dry Sliding, Water- and Oil-Lubricated Conditions," *Tribology Letters*, **45**, pp 1–7.

(15) Kim, B. C., Park, D. C., Kim, B. J., and Lee, D. G. (2010), "Through-Thickness Compressive Strength of a Carbon/Epoxy Composite Laminate," *Composite Structures*, **92**, pp 480–487.

(16) Kim, S. S., Lee, H. G., and Lee, D. G. (2005), "Tribological Behaviors of Carbon Composite Grooved Surfaces," *Composite Structures*, **71**, pp 238–245.

(17) ASTM International. (2010), "Standard Test Method for Linearly Reciprocating Ball-on-Flat Sliding Wear Designation," **ASTM Standard G133-05**.

(18) Zhang, D. Y., Lin, P., Dong, G. N., and Zeng, Q. F. (2013), "Mechanical and Tribological Properties of Self-Lubricating Laminated Composites with Flexible Design," *Materials & Design*, **50**, pp 830–838.

(19) Zhang, W., Li, X., and Yang, R. (2011), "Pyrolysis and Fire Behaviour of Epoxy Resin Composites Based on a Phosphorus-Containing Polyhedral Oligomeric Silsesquioxane (Dopo-Poss)," *Polymer Degradation and Stability*, **96**, pp 1821–1832.

(20) Biswas, S. and Satapathy, A. (2010), "A Study on Tribological Behavior of Alumina-Filled Glass–Epoxy Composites Using Taguchi Experimental Design," *Tribology Transactions*, **53**, pp 520–532.

(21) Öztürk, B., Arslan, F., and Öztürk, S. (2013), "Effects of Different Kinds of Fibers on Mechanical and Tribological Properties of Brake Friction Materials," *Tribology Transactions*, **56**, pp 536–545.

(22) Li, D. X., You, Y. L., Deng, X., Li, W. J., and Xie, Y. (2013), "Tribological Properties of Solid Lubricants Filled Glass Fiber Reinforced Polyamide 6 Composites," *Materials & Design*, **46**, pp 809–815.

(23) Meng, H., Sui, G. X., Xie, G. Y., and Yang, R. (2009), "Friction and Wear Behavior of Carbon Nanotubes Reinforced Polyamide 6 Composites under Dry Sliding and Water Lubricated Condition," *Composites Science and Technology*, **69**, pp 606–611.

(24) Liza, S., Haseeb, A., Masjuki, H. H., and Abbas, A. A. (2012), "The Wear Behaviour of Cross-Linked UHMWPE under Dry and Bovine Calf Serum-Lubricated Conditions," *Tribology Transactions*, **56**, pp 130–140.

(25) Zhang, L., Xiao, J., and Zhou, K. (2012), "Sliding Wear Behavior of Silver–Molybdenum Disulfide Composite," *Tribology Transactions*, **55**, pp 473–480.

(26) Hu, T. C., Zhang, Y. S., and Hu, L. T. (2012), "Tribological Investigation of MoS_2 Coatings Deposited on the Laser Textured Surface," *Wear*, **278**, pp 77–82.

(27) Dong, G. N., Hua, M., Li, J., and Chuah, K. B. (2007), "Temperature Field and Wear Prediction for UHMWPE Acetabular Cup with Assumed Rectangular Surface Texture," *Materials & Design*, **28**, pp 2402–2416.

(28) Zhang, R., Guessous, L., and Barber, G. C. (2012), "Investigation of the Validity of the Carslaw and Jaeger Thermal Theory under Different Working Conditions," *Tribology Transactions*, **55**, pp 1–11.

(29) Mu, L. W., Shi, Y. J., Feng, X., Zhu, J. H., and Lu, X. H. (2012), "The Effect of Thermal Conductivity and Friction Coefficient on the Contact Temperature of Polyimide Composites: Experimental and Finite Element Simulation," *Tribology International*, **53**, pp 45–52.

(30) Laraqi, N., Alilat, N., de Maria, J. M., and Baïri, A. (2009), "Temperature and Division of Heat in a Pin-on-Disc Frictional Device—Exact Analytical Solution," *Wear*, **266**, pp 765–770.